Statistical methods for electromagnetic induction imaging with atomic magnetometers.

Prova di Statistica del corso di dottorato in fisica sperimentale XXXV° ciclo
Dipartimento di scienze fisiche, della terra e dell'ambiente
Università di Siena

Prof: Paolo Francavilla

Studente: Alessandro Fregosi

1 Introduction

Electromagnetic induction imaging consists in obtaining a map of a quantity related to the electric permittivity ϵ, the magnetic permeability μ or the electric conductivity a σ of an object. A variety of different techniques are used to acquire these images, one of the first example is [1]. Here we focus on a image acquired using a radio-frequency cold atom magnetometer. In this case, a cloud of cold ^{85}Rb atoms, released from a MOT at a temperature T~100μK, are optically pumped along a static bias magnetic field $\vec{B}_0 = B_0\hat{x}$ in the ground state of maximum magnetic moment. An oscillating magnetic field $\vec{B}_{RF} = A\cos(\omega t + \alpha)\hat{z}$ orthogonal to $\vec{B}_0$ induces the Larmor precession of the polarized atoms with angular frequency $\omega_0 = \gamma B_0$ (γ is the gyromagnetic factor) hence a transverse polarization S_x, oscillating with an angular frequency ω_0, is generated. This transverse polarization induces the Faraday rotation of the linear polarization of a probe laser beam that is detected with a polarimeter whose output is a time depending signal that, in the steady state, can be written as [2]:

$$s(t) = \frac{1}{2}S_0 B_{\mathrm{RF}} \frac{T_2\cos(\omega t + \alpha) + (\omega - \omega_0)T_2^2 \sin(\omega t + \alpha)}{1 + (\gamma B_{\mathrm{RF}}/2)^2 T_1 T_2 + (\omega - \omega_0)^2 T_2^2} \tag{1}$$

where T_1 and T_2 are respectively the longitudinal and transverse lifetimes of the spin polarization. Defining $\delta = (1/T_2)\sqrt{1 + (\gamma B_{RF}/2)^2 T_1 T_2}$ and casting all the multiplicative factors in one costant A eq. 1 can be written as

$$s(t) = A\frac{\delta\cos(\omega t + \alpha) + (\omega - \omega_0)\delta T_2 \sin(\omega t + \alpha)}{\delta^2 + (\omega - \omega_0)^2} \tag{2}$$

The lock-in amplifier multiplies the signal in eq. 1 by $\cos(\omega t + \phi)$ and $\sin(\omega t + \phi)$ and integrate the results of the multiplication over a time longer than the period of the oscillation (the phase ϕ can be chosen arbitrarily) . The results are two signals: the in-phase component i.e. the term proportional to $\cos(\omega t)$ and the in-quadrature component i.e. the term proportional to $\sin(\omega t)$ called respectively the x and y channels (chx and chy). The chx and chy channels can then be written as:

$$\mathrm{chx}(\phi) = \frac{A}{2}\frac{\delta\cos(\alpha - \phi) - (\omega - \omega_0)\delta T_2 \sin(\alpha - \phi)}{(\omega - \omega_0)^2 + \delta^2} \tag{3}$$

$$\mathrm{chy}(\phi) = -\frac{A}{2}\frac{\delta\sin(\alpha - \phi) + (\omega - \omega_0)\delta T_2 \cos(\alpha - \phi)}{(\omega - \omega_0)^2 + \delta^2} \tag{4}$$

Changing the phase ϕ the chx and the chy channels can be exchanged, but two new terms can be constructed: the amplitude channel:

$$\mathrm{amp} = \sqrt{chx^2 + chy^2} = \frac{A}{2}\frac{\sqrt{\delta^2 + (\omega - \omega_0)^2\delta^2 T_2^2}}{(\omega - \omega_0)^2 + \delta^2} \tag{5}$$

and the phase channel. The amplitude channel is independent by the difference $(\alpha - \phi)$.

If $\alpha = \phi$ the chx channel has the form:

$$\mathrm{chx}(\omega) = \frac{A}{2}\frac{\delta}{\delta^2 + (\omega - \omega_0)^2} \tag{6}$$

that is proportional to a Cauchy distribution.

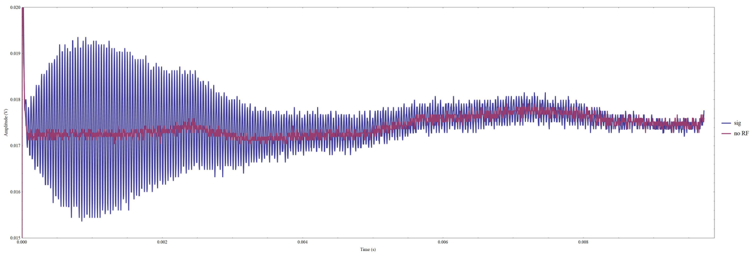

Figure 1: An example of the signal recorded from the polarimeter.

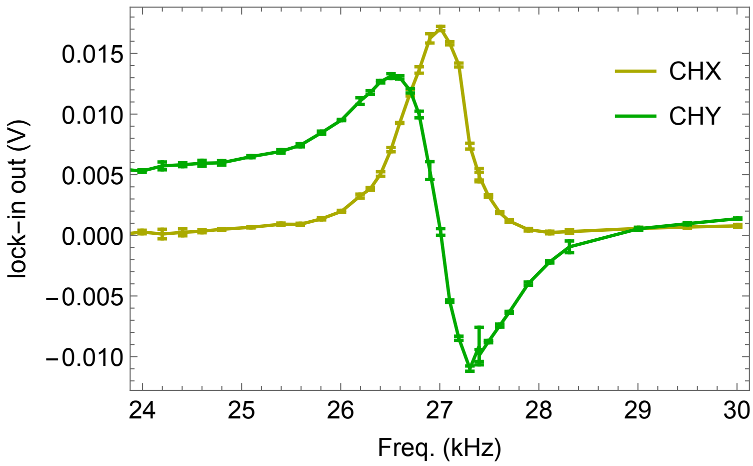

Figure 2: An example of the two channels of the lock-in as a function of ω.

If a conducting object is placed in between the source of $\vec{B}_{RF}$ and the atoms, the total magnetic field at the cloud position is the sum of $\vec{B}_{RF}$ and $\vec{B}_{EC}$, the field produced by the eddy currents induced on the object by $\vec{B}_{RF}$ itself and the total magnetic field changes in both amplitude and phase with respect to $\vec{B}_{RF}$. If these changes are recorded while the object is moved in the $x - y$ plane over the MOT an electromagnetic induction image can be recorded.

2 Magnetometer characterization

In fig. 1 is reported an example of the signal produced by the polarimeter, as it can be seen, the amplitude of the signal decays in time as a consequence of, among other factors, the expansion and fall of the atoms. In this situation the equations eq. 3 and eq. 4 are no longer time independent and the channels of the lock-in amplifier are averaged over the acquisition time. In order to characterize the magnetometer, the output of the two channels of the lock-in are recorded as a function of the angular frequency ω of $\vec{B}_{RF}$. In particular, if $(\alpha - \phi) = 0$, the chx channel output should have a shape given by eq. 3 that is proportional to a Cauchy distribution and that permits to find the central frequency and the width of the magnetic resonance.

A Cauchy probability density function is determined by two parameters: the location parameter ω_0 and the scale parameter δ. This p.d.f. has infinite mean and variance and does not have sufficient statistics for its parameters. Despite that we have to find the width of the

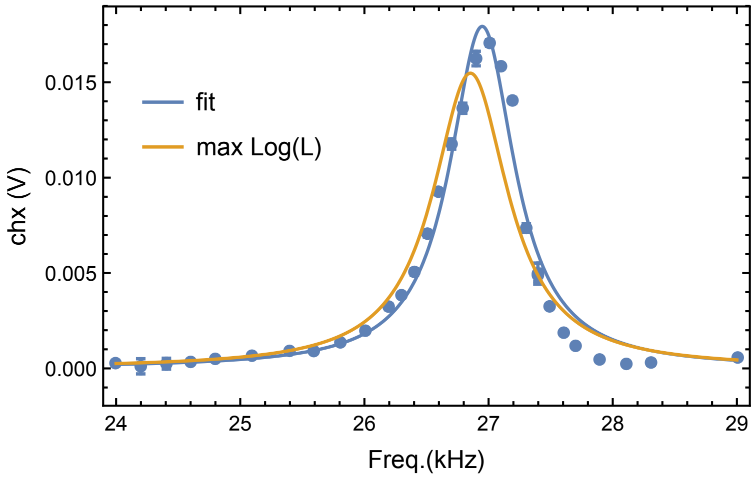

Figure 3: An example of the two channels of the lock-in as a function of ω.

magnetic resonance and its resonance frequency in order to characterize the magnetometer, so we have to determine both the scale parameter and the location of the Cauchy distribution eq. 3.

An example of the data acquired form both the chx and chy channels of the lock-in amplifier is reported in fig. 2. Each point is the average over 5 acquisitions, the values on the x axis (the frequencies) are considered exact while the errors on the y axis are estimated calculating the standard deviation of the 5 measurements.

In order to determine the resonance frequency and the width of the magnetic resonance, we used a commercial mathematical software that has a built-in function for calculating the fit of a curve. The results obtained by an unweighted fitting procedure using the function in eq. 3 are: $A = 0.0179$, $\delta = 1.274$, $\omega_0 = 26.949$. An example of the resulting fit superimposed to the data is reported in fig. 3 where it can be seen that the fitted curve doesn't represent exactly the data. In order to determine how far the curve is from the experimental data3 we calculate the statistics

$$s = \sum_{i=1}^{n} \left(\frac{y_i - f(x_i)}{\delta y_i} \right)^2 = 1491 \tag{7}$$

This statistics is distributed according to a χ^2 distribution with 35 degree of freedom (we had 38 points and we determined three parameters) and the probability of obtaining a smaller value of s is by the integral of χ^2_{35} between 0 and 1491 giving 1.

As an alternative way of finding a fitting function for the data we used the likelihood. The likelihood L is the probability of obtaining the measured data given the value of the parameter. Assuming that the measures are independent we have $L(\mu, \delta) = \prod_{i=1}^{n} f(x_i|\mu, \delta)$ and is usually used the logarithm of the likelihood

$$\log L = \sum_{i=1}^{n} \log f(x_i|\mu, \delta). \tag{8}$$

The values of δ and ω_0 that will be choosen are the ones for which $\log L$ as a maximum (the A parameter of eq. 3 is set to 1).

The maximum likelihood method can be problematic for a Cauchy distribution, but in the case where both the parameters have to be determined it has been proven [3] that the

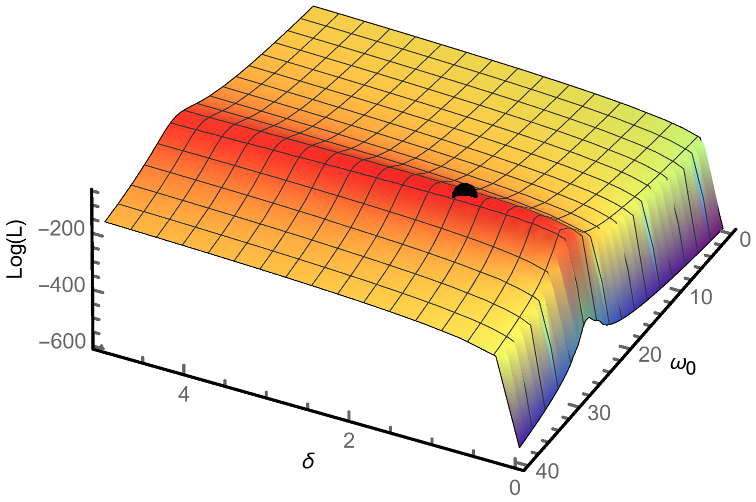

Figure 4: Graph of $\log L(\mu, \delta)$ with the maximum found (the black dot).

likelihood has an unique stationary point. The graph of $\log L$ over a reasonable interval for the parameters is reported in fig. 4 together with the maximum found with the mathematical software. The resulting values found are $\delta = 1.476$ and $\omega_0 = 26.854$.

The graph of the fitted function with these parameters is reported in fig. 3. Also in this case we calculated the χ^2 test resulting in $s = 3142$ and again the probability of finding a smaller value of s is 1.

3 Analysis of an image background noise

In order to obtain an electromagnetic induced image of a conducting object we set the frequency of $\vec{B}_{RF}$ at the peak of the magnetic resonance (determined by the constant magnetic field $\vec{B}_0$) found using the methods described in the previous section. When the magnetometer is set, we record the value of the amplitude channel of the lock-in amplifier as a function of the position of the object under examination maintaining fixed the frequency of $\vec{B}_{RF}$. Given that the eddy currents induced on the object generate an alternating magnetic field opposite to $\vec{B}_{RF}$ we expect that the amplitude is reduced if the object is placed between the $\vec{B}_{RF}$ source and the MOT.

In fig. 6 is reported the image of a 30×30×7 mm^3 copper object. It can be seen that in correspondence of the object the amplitude of the magnetometer response is actually reduced. The points at the border of the image (in black) where the object is not interposed in between the $\vec{B}_{RF}$ source and the atoms, are used to analyze the background noise.

The amplitude of the magnetometer response depends on various factors. For example the ambient magnetic field could change, resulting in a different value of $\vec{B}_0$, hence in a different resonance frequency and in eq. 5 it can be seen that the amplitude is maximum at resonance. Another cause can be a different number of atoms trapped in the MOT caused by various factors as casual misalignment of the lasers or variations of the lasers frequencies. . . etc. In order to reduce the fluctuations of the system we divide the value of the recorded amplitude

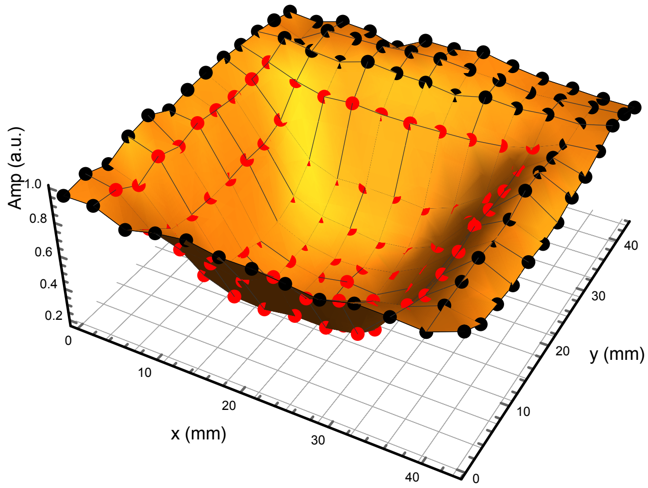

Figure 5: The image in exam: the dots (red and black) are the points at which the measurements are done, the black dots are those used for the background noise analysis.

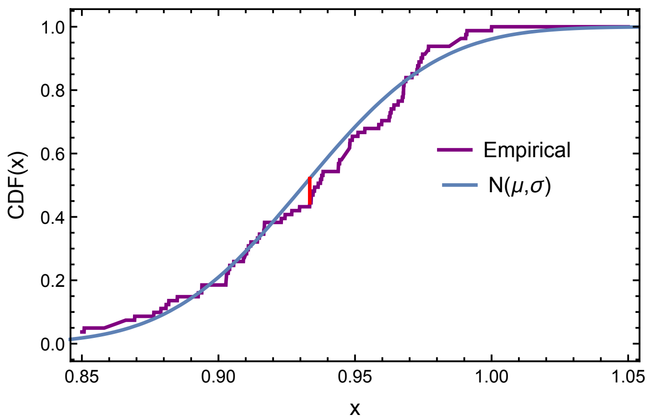

Figure 6: The cumulative distribution of the empirical distribution and the normal distribution. The vertical red line is the maximum of $d_n(x_i)$.

by a number proportional to the fluorescence light emitted by the MOT, in fact, from eq. 1, we see that the signal amplitude is proportional to the polarization S_x that is due to the number of polarized atoms interacting with the lasers, and the fluorescence light emitted by the atoms is again proportional to the number of atoms in the MOT.

In order to verify if the system is stable over the period of time necessary to obtain an image, we made the assumption that the fluctuations of the amplitude are distributed according to a normal distribution. This distribution is sampled in the $n = 81$ points at the border indicated by balck dots in fig. 6. So we made a Kolomorov-Smirnov test for the H_0 hypothesis: data are distributed according to a normal distribution [5]. The data used for this test are the ones at the border of fig. 6 where we assume that the object is far from the MOT so that this points can be used as a zero measure.

Given that the mean ad variance of the distribution are unknown, they have to be

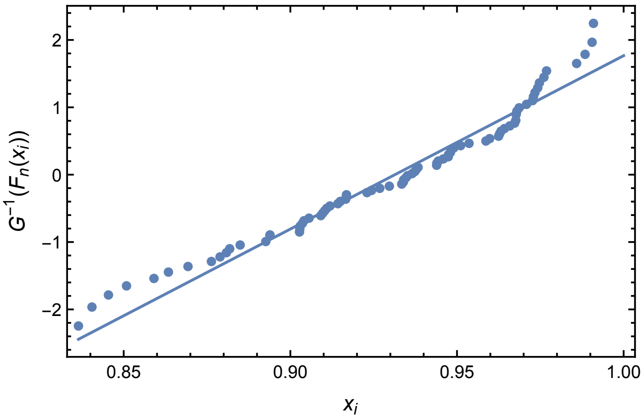

Figure 7: Probability plot of the cumulative empirical distribution.

estimated by the data:

$$\mu = \frac{1}{N}\sum_{i=1}^{N} x_i = 0.931 \qquad s^2 = \frac{1}{N-1}\sum_{i=1}^{N}(x_i-\mu)^2 = 0.001509 \tag{9}$$

Posing $F_n(x)$ the cumulative empirical distribution and $F(x)$ the cumulative normal distribution with mean and variance calculated using eq. 9 we obtain that the maximum distance between F_n and F is:

$$d_n = \sup_n \left\{ \left|F(x_i) - F_n(x_i)\right|, \left|F(x_i) - F_n(x_{i-1})\right| \right\} = 0.08898 \tag{10}$$

Since we have estimated the mean and variance of the distribution from the sample, the statistic t must be evaluated using [4].

$$t = d_n\left(\sqrt{n} - 0.01 + \frac{0.85}{\sqrt{n}}\right) = 0.808356. \tag{11}$$

The p-value can be calculated using the asymptotic Kolomorov distribution:

$$\mathrm{p-value} = 2\sum_{k=1}^{\infty}(-1)^{k+1}e^{-2k^2t^2} \tag{12}$$

resulting in p=0.531 meaning that the H_0 hypothesis can't be rejected. This calculation is not entirely correct because eq. 12 can't be used when the mean and variance of the distribution are calculated from the data. For this case, the value of t corresponding to the 0.05 significance is tabulated in [4] as $t = 0.895$ that is greater than the value we found meaning that the hypothesis can't be rejected.

A further evaluation can be done with a normal plot from the expression of the cumulative distribution:

$$F(x) = \frac{1}{\sqrt{2\pi}\sigma}\int_{-\infty}^{x} \mathrm{e}^{-\frac{(y-\mu)^2}{2\sigma^2}}\,\mathrm{d}y \tag{13}$$

after changing variable we obtain:

$$z = \frac{x-\mu}{\sigma} \rightarrow G(z) = \frac{1}{\sqrt{2\pi}}\int_{-\infty}^{z} \mathrm{e}^{\frac{y^2}{2}}\,\mathrm{d}y \tag{14}$$

and

$$G^{-1}\Big(F(x)\Big) = G^{-1}\Big(G(z)\Big) = z = \frac{x-\mu}{\sigma}. \quad (15)$$

The points $\left(x_i, G^{-1}(F(x_i))\right)$ are on the line $y = \frac{x-\mu}{\sigma}$.

Given that the empirical distribution converges to the true distribution, if in eq. 15 we substitute $F(x)$ with $F_n(x_i)$, we can see how the points $\left(x_i, G^{-1}(F_n(x_i)\right)$ are placed with respect to the line in eq. 15. This graph is reported in fig. 7 where it can be seen that the points at the left and right extremes are those at a greater distance from the normal line.

4 Conclusion

The analysis of the fit procedures for the Cauchy distribution in sec. 1 revealed that the results obtained are rather poor. Although this result can be due to the underestimation of the errors in the lock-in output in fig. 3, considering eq. 3 and eq. 4 we see how the shapes of the curve are determined by the difference $(\alpha - \phi)$ but α is the phase angle of the magnetic field $\vec{B}_{RF}$ while the lock-in amplifier acquires the phase of the current that generates $\vec{B}_{RF}$, given that the experiment is mounted over conducting optical tables this can introduce a frequency dependent phase lag in $\vec{B}_{RF}$ compared to the current resulting in a poor adaptation of the curve to the data.

From the analysis of the background of an image in sec. 2 it can be concluded that there are no reasons to confute the hypothesis that the data are normally distributed although there are some points, at the extremes in fig. 7, far from the line that indicates that are normally distributed. Given that data are already normalized over the number of atoms captured in the MOT, the reason for this discrepancy should be searched in the optical pumping process. In any case the estimate of the variance of the distribution, combined with the techniques in [5], will provide a sound starting point for an evaluation of the resolution achievable for images of more complicated objects.

References

[1] A. Wickenbrock et. al. *Magnetic induction tomography using an all-optical ^{87}Rb atomic magnetometer*. Opt. Lett. 2014, 39, 6367.

[2] S. J. Seltzer *Developments in Alkali-Metal atomic magnetometry* Phd Thesis 2008.

[3] J. B. Copas *On the unimodality of the likelihood for the Cauchy distribution* Biometrika, 62, 701-704. (1975)

[4] D'Agostino R. B. and Stephens M. A. *Goodness of fit techniques* (1986).

[5] N. Papi et. al. *Edge detection in atomic magnetometer imaging* JSAS Vol. 10 No. 1 (2018)